Thermochimica Acta, 41 (1980) 335—355
Elsevier Scientific Publishing Company, Amsterdam — Printed in Belgium

THERMAL AND MOSSBAUER STUDIES OF IRON-CONTAINING HYDROUS SILICATES. II. HISINGERITE

K.J.D. MACKENZIE and R.M. BEREZOWSKI

Chemistry Division, Department of Scientific and Industrial Research, Private Bag, Petone (New Zealand)

(Received 15 April 1980)

ABSTRACT

Thermal analysis, X-ray diffraction, IR and Mossbauer studies of the thermal reactions of three hisingerites of varying manganese content suggest that the unheated materials, although very poorly crystalline, contain elements of structure with characteristics similar to an iron-rich, probably dioctahedral, smectite. The presence of chlorite in one of the samples is not a prerequisite to the structure. On heating, water is lost in two well-defined stages during which the hisingerite "structure" is maintained but the ferric sites suffer increased distortion from octahedral symmetry. In air, the higher-temperature recrystallization products are SiO_2 and iron oxide or iron—manganese spinel, depending on the starting composition, while under reducing conditions, iron metal and ferrous or ferromanganese silicates are formed.

INTRODUCTION

Hisingerite is a semi-amorphous or very poorly crystalline hydrous iron silicate of variable composition, first described by Berzelius, who named it after a co-worker, W. Hisinger. The type material (Table 1A, column 4) was an alteration product occurring in reniform masses associated with pyrite in a copper mine at Riddarhyttan, Sweden [1]. Manganese-rich varieties of the mineral are not uncommon; these were earlier called manganhisingerites but the name more favoured today is neotocite (Greek: "of recent origin").

Although these minerals were originally described as amorphous, improvements in X-ray and electron diffraction techniques have revealed several broad, diffuse bands indicating at least some regions of low crystallinity [2—8]. This has led to the suggestion that hisingerite is either a mixture of poorly crystallized material in an amorphous matrix [2,3], a single poorly crystallized phase [4—6], or a mixture of two or more fine-grained crystalline phases [7]. The identity of the crystalline phase has given rise to difference of opinion: Gruner [8] favoured a smectite, possibly nontronite, on the basis of the similarity of the few broad X-ray lines with some of the major nontronite spacings. Golubova et al. [5] have also assigned a layer-lattice montmonillonite-group structure to a Russian hisingerite, while more recently a Japanese hisingerite has been described as a very poorly crystallized nontronite [6]. This structural assignment is, however, far from conclusive, since the diagnostic basal spacing is rarely observed, thus precluding positive identification by glycolation. Dietrich [3] attempted to glycolate

hisingerite, but reported no change in any of the "nontronite" X-ray peaks. Furthermore, no DTA endotherm has previously been reported at about 500°C in hisingerite, such as occurs during nontronite dehydroxylation, although Dietrich [3] has suggested that a small endotherm/exotherm structure might be due to the loss of hydroxyl water and a similar claim has been made by Kohyama and Sudo [6] for an almost indistinguishable inflexion at about 400—500°C in their DTA curve.

Whelan and Goldich [7] pointed out that the chemical analyses of some of their hisingerites could be accommodated by a trioctahedral smectite structure approaching an iron-rich saponite composition, but other samples contained too much iron for such a structure. The suggestion that the excess iron occurs as goethite is not supported by DTA or X-ray diffraction of these samples [7]. Furthermore, the calculated saponite structure was achieved by the false assumption that the iron is ferrous, even though the iron in hisingerite is known to be principally ferric.

An alternative view was taken by Lindqvist and Jansson [4] who pointed out that the chemical analyses of many hisingerites could correspond with an interstratified montmorillonite/chlorite in the ratio of about 2 : 1. They suggested [4] that the analyses would also be fitted by a mica structure, which would provide an explanation for the absence of the basal spacing, since in the mica structure, the opportunity exists for extensive tetrahedral substitution of Fe for Si, leading to extremely poorly ordered layer stacking.

Several authors have discussed the relationship between the semi-crystalline phase of hisingerite and a crystalline phase of composition $2\ SiO_2 \cdot Fe_2O_3 \cdot n\ H_2O$ named canbyite [2,9,10] which has a similar composition and X-ray pattern and has led to the suggestion [10] that canbyite is simply well-crystallized hisingerite.

The thermal behaviour of hisingerite and neotocite is known mainly through DTA studies. The high-temperature products have been variously described as "a spinel and one of the high-temperature modifications of silica" [3], "ferrites" [4,7] or hematite and cristobalite [6]. Neotocite behaves similarly, but the firing product is usually braunite ($MnO \cdot 3\ Mn_2O_3 \cdot SiO_2$) [4,7,12]. Published IR spectra of hisingerite and neotocite [5—7,12,13] show broadly similar features to nontronites. No Mossbauer spectra have been reported.

The aim of this work is to investigate the thermal reactions of three members of the hisingerite—neotocite series, using a range of techniques as in a previous study of nontronites [11], in the hope that a comparison of the thermal behaviour of the two mineral types under oxidizing and reducing conditions might provide further information about the relationship between hisingerite and the better-characterised layer-lattice minerals.

EXPERIMENTAL

Materials

Three minerals were studied; the first, designated H1, is from the Gillinge Mine, Sodermanland County, Sweden and has been described as neotocite by

Lindqvist and Jansson [4]. The present sample was from specimen 400/4 of the Uppsala University collection, where it is catalogued as gillingite. X-Ray powder diffraction indicated that the as-received sample contained a trace of magnetite and pyrite impurity, but otherwise showed the three broad featureless bands centred at about 3.6, 2.55 and 1.55 Å, characteristic of hisingerite. A weak X-ray band at about 8 Å may indicate the presence of a trace of chlorite. The sample used for further study was separated from the magnetite impurity by magnetic separation, and the chemical analysis of the purified material is shown in Table 1A, column 1.

The second sample, designated H2, was a brownish material from the Potosi Mine, Santa Eulalia, Mexico, being part of specimen 95905 of the mineral collection, Smithsonian Institution, Washington. This sample was less crystalline than H1, its X-ray trace showing only two very weak, broad features at about 2.6 and 1.55 Å and several small but sharp impurity peaks corresponding reasonably well with alleghanyite, $Mn_5(OH)_2(SiO_4)_2$ (JCPD Card 25-1183). The chemical analysis (Table 1A, column 2) shows it to contain appreciably more manganese than can be accounted for by the manganese-containing impurity; this material therefore appears to be intermediate between a high-manganese neotocite and a ferric hisingerite.

The third sample, H3, is a true ferric hisingerite occurring in iron ore from the Solberg Mine, Grythyttan, Orebo County, Sweden, from sample 400/2 of the mineral collection of the Mineralogical—Petrological Institute of the

TABLE 1A

Chemical analyses and unit cell contents of hisingerites

Component	1	2	3 *	4
SiO_2	34.21	32.19	35.24	35.02
Al_2O_3	0.97	0.00	2.00	1.20
Fe_2O_3	18.68	27.20	35.51	39.46
FeO	1.55 **	2.03 **	2.40	2.20
MnO	20.74	13.19	0.34	
TiO_2	0.00	0.03	0.00	
MgO	3.22	0.39	3.77	0.80
CaO	1.06	0.71	1.99	Tr
Na_2O	0.05	0.67	0.00	
K_2O	0.11	0.15	0.04	
H_2O^+	9.13 ***	11.58 ***	10.42	11.20
H_2O^-	9.53	12.72	9.03	10.50
Total	99.25	100.86	100.74	100.38

Column 1: Sample H1, neotocite (gillingite), Sweden. Analyst: J.E. Patterson.
Column 2: Sample H2, hisingerite, Mexico. Analyst: A. Cody.
Column 3: Sample H3, hisingerite, Sweden. Analysts: B. Almqvist and B. Lindqvist.
Column 4: Hisingerite, type material, Riddarhyttan, Sweden. Analysts: P.T. Cleve and A.E. Nordenskiold (1866).
* Sample H3 as used in present study also contained ~12% hematite (estimated by Mossbauer spectroscopy.
** FeO content estimated by Mossbauer spectroscopy.
*** Below 130°C.

TABLE 1B

Unit cell contents

		H1 *		H2 *		H3 *		H1 **		H2 **		H3 **	
Si	Td	6.46	8.0	6.44	8.0	6.26	8.0	6.08	8.0	5.88	8.0	5.80	8.0
Al		0.22				0.42		0.20				0.38	
Fe^{3+}		1.32		1.56		1.32		1.72		2.12		1.82	
Fe^{3+}	Oh	1.34	5.84	2.52	5.22	3.42	4.84	0.78	5.02	1.60	4.06	2.56	3.86
Fe^{2+}		0.24		0.34		0.36		0.23		0.31		0.32	
Mg		0.90		0.12		1.00		0.85		0.11		0.93	
Mn		3.36		2.24		0.06		3.16		2.04		0.05	
Ca	Exch.	0.43	0.47	0.30	0.60	0.75	0.76	0.41	2.71	0.27	4.02	0.70	3.19
K		0.02		0.26		0.01		0.02		0.03		0.01	
Na		0.02		0.04				0.02		0.24			
H_3O^+								2.26		3.48		2.48	
O		20		20		20		20		20		20	
(OH)		4		4		4		4		4		4	

* Calculated on a smectite model by the method of Ross and Hendricks [17].

** Calculated on a hydromica model by the method of Brown and Norris [18].

University of Uppsala, Sweden. This material has been fully described by Lindqvist and Jansson [4]. The principal impurity was shown by X-ray diffraction to be hematite, most of which could be removed by heavy liquid separation in a medium of density 2.95. However, a better yield of the non-hematite fraction was obtained by cutting the sample at a density of 3.3, and although the separation of hematite was then less complete, this compromise was adopted. A fairly strong but broad X-ray peak at d = 7.31 Å was noted; this was attributed by Lindqvist and Jansson to chlorite in intimate relationship with the hisingerite. The chemical analysis is shown in Table 1A, column 3.

Methods

Because of the small amounts of purified sample available, a serial heating method was used, in which the sample was heated to the lowest temperature for 0.5 h, cooled and examined by X-ray diffraction, IR and Mossbauer spectroscopy, then returned to the furnace and re-heated to the next temperature. The temperatures were chosen from the DTA traces run at 10° C min^{-1} under air, oxygen-free nitrogen and hydrogen—nitrogen mixture (5% H_2/95% N_2). Firings of all three hisingerites were made in air and H_2/N_2 for the X-ray—IR—Mossbauer work, and sufficient sample H2 was available for a full study of that material in oxygen-free nitrogen also. The IR spectra were obtained on a Perkin-Elmer-580 spectrophotometer, the samples being at 0.3% concentration in KBr discs. Details of the X-ray diffraction and Mossbauer spectroscopy appear elsewhere [11]. TG runs were made under oxygen-free nitrogen (4.0 ml min^{-1}) at a heating rate of 10° C min^{-1} on a Stanton TG770 thermobalance.

RESULTS AND DISCUSSION

Chemical analyses

The chemical analyses of hisingerites H1, H2 and H3 are given in Table 1A and, for comparison, some typical analyses of other crystalline minerals which have been suggested as structural types are given in Table 2.

Comparison of Tables 1 and 2 shows distinct similarities between the present hisingerites and nontronite, the structure of which is able to accommodate the ferric iron content typical of hisingerite. The analysis of a Russian hisingerite described by Golubova et al. [5] as a new mineral of dioctahedral smectite structure has been included in Table 2 because of its clear identity with nontronite, confirmed by the presence of a 13.46 Å basal spacing. The trioctahedral saponite structure suggested by Whelan and Goldich [7] is less able to accommodate the high Fe^{3+} content of hisingerite, and even the unusual high-iron example shown in Table 2 (column 3) contains considerably more Mg than occurs in the hisingerites. Additional iron could be incorporated in the saponite structure if it were in the ferrous form, by replacement of Mg, but Mossbauer evidence (see later) rules out this possibil-

TABLE 2

Chemical analyses and numbers of ions in unit cells of minerals possibly related to hisingerite

Element	Nontronite [11]	Bakchar hisingerite [5]	Iron-rich saponite [14]	Iron-rich saponite [15]	Iron-rich hydromuscovite [16]
SiO_2	38.76	32.62	39.68	46.05	46.32
Al_2O_3	5.45	2.94	3.93	13.57	28.79
Fe_2O_3	29.25	40.36	19.82	9.15	5.74
FeO	0.15	5.52	1.12	1.56	1.50
MnO	0.03			0.14	
TiO_2	0.21				0.03
MgO	0.67		11.21	4.32	Tr
CaO	1.55	1.97	2.37	1.99	1.09
Na_2O	0.17			1.71	0.00
K_2O				0.36	9.31
H_2O	18.86	15.24	21.27	21.17	6.16
Unit cell contents					
Td Si	6.86	6.30	6.78	7.32	6.36
Td Al	1.14	0.66	0.78	0.68	1.64
Td Fe^{3+}		1.04	0.44		
Td *	8.0	8.0	8.0	8.0	** 8.0
Oh Fe^{3+}	3.90	3.38	2.10	1.08	0.59
Oh Fe^{2+}	0.02	0.90	0.16	0.22	0.17
Oh Al				1.86	3.02
Oh Mg	0.32	0.18	2.84	1.02	
Oh Mn			0.02	0.02	
Oh Ca				0.34	0.16
Oh	4.29	4.46	5.12	4.54	3.94
Exch. Ca	0.53	0.40	0.86		
Exch. K		0.04		0.08	1.63
Exch. Na	0.05	0.06		0.52	
Exch. H_3O^+		0.22			0.44
Exch.	0.66	0.72	0.86	0.60	2.07
O	20	20	20	20	20
(OH)	4	4	4	4	4

* Recalculated by Ross and Hendrick's method [17].
** Calculated by Brown and Norrish's method [18].

ity. Furthermore, substitution in saponite usually occurs in the tetrahedral rather than octahedral sites (ref. 16, p. 230). Another iron-rich saponite suggested to be a precursor of hisingerite [15] (Table 2, column 4) bears only slight compositional similarities to the present hisingerites which are relatively low in Si and Al. The low Si and Al contents also present difficulties in realizing a typical hydromica structure (Table 2, column 5) unless very extensive substitution by Fe^{3+} is postulated [4]. Calculations of the until cell contents of the present hisingerites on the basis of both smectite and hydromica structures are included in Table 1B. Reasonable fits to both smectite

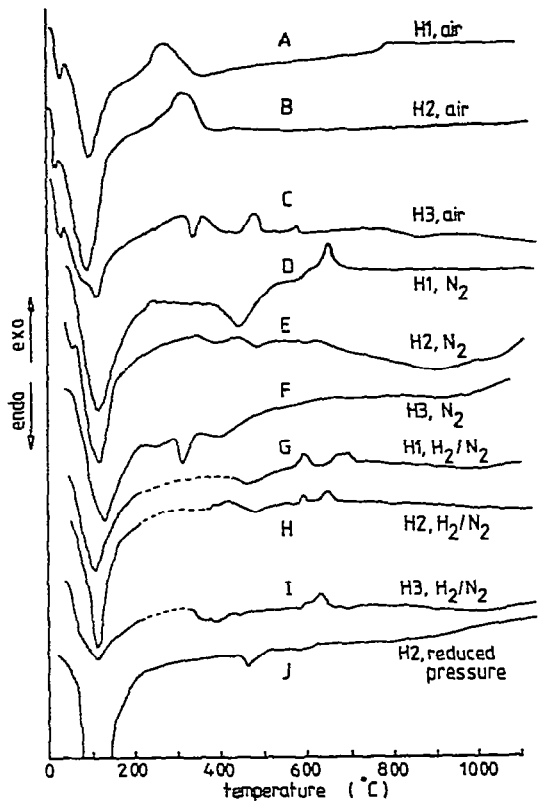

Fig. 1. DTA traces of hisingerites. Heating rate: 10°C min^{-1}. Dashed portions of curves G,H and I indicate regions where background curves were subtracted to eliminate noise due to adsorption of H_2 by the platinel thermocouples.

and hydromica models are obtained, illustrating the inadvisability of making structural distinctions on the basis of chemical analyses alone.

Thermal analyses

The DTA traces of the three samples under different atmospheres are shown in Fig. 1. Some variations occur in the traces, but the following general features can be distinguished.

(i) A large endotherm at about 100°C in all samples under all atmospheres, corresponding to the loss of loosely-bound water. This feature occurs in all previously published DTA traces [2,3,6,7,12].

(ii) Another endotherm at 350—480°C in all samples under all atmospheres. The peak temperature and shape is extremely atmosphere-dependent, it being broader and displaced to lower temperatures in air, suggesting the removal of more tightly-bound water possibly occurring in coordination with the iron and manganese. A small endotherm has been reported by Dietrich [3] at about this temperature, and a less obvious feature was also commented on by Kohyama and Sudo [6] in a study on a Japanese hisingerite, but other published DTA traces do not show this peak. Because of the significance of this exotherm for structural considerations, and since it is difficult to observe in air, the DTA trace of sample H2 was obtained under

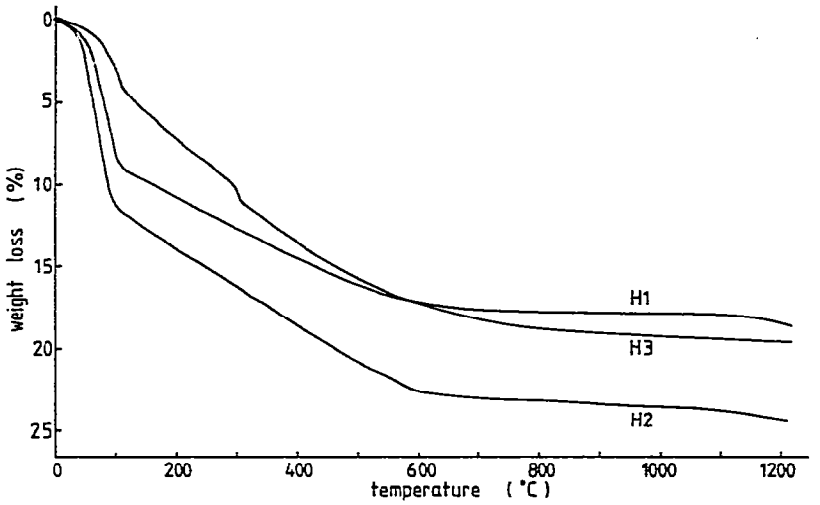

Fig. 2. TG curves of hisingerites. Heating rate: 10°C min^{-1}; atmosphere: oxygen-free nitrogen, 4.0 ml min^{-1}.

reduced pressure (Fig. 1J). This gives the clearest possible indication of the existence of the endotherm. Insufficient sample prevented similar experiments being made on H1 and H3.

(iii) Sundry exotherms, varying with atmosphere and starting material. In H1 a small peak occurs in air at ~800°C, but in N_2 it is of increased intensity, and displaced to 650°C. X-Ray diffraction (see following section) indicates that this represents the formation of jacobsite ($MnFe_2O_4$) and/or braunite ($MnO \cdot 3\,Mn_2O_3 \cdot SiO_2$). Under reducing conditions, at least two peaks occur, corresponding to the formation of an olivine and a pyroxene. The higher-temperature exotherms are not obvious in H2, except in H_2/N_2, where they again appear as twin peaks. There is little evidence of the exotherms reported by Clark et al. [12] in a series of neotocites and attributed to the oxidation of Mn^{2+} to Mn^{3+}. In sample H3, the main exotherm occurring at about 450°C in air is unaccompanied by any appearance of new phases in the X-ray trace, and is probably due to the oxidation of pyrite impurity, particularly since it is absent under non-oxidising conditions. Under H_2/N_2 a partially-resolved exotherm at about 620°C is analogous to the double exotherms in H1 and H2, and is related to olivine formation.

The TG traces for all three hisingerites under oxygen-free nitrogen are shown in Fig. 2. All three samples show an initial rapid weight loss up to ~130°C due to the loss of loosely-bound water, followed by a more gradual loss up to 600—700°C due to loss of more tightly-bound water. Some evidence for a multistage process is apparent in sample H3, the sharp inflexion at 300°C coinciding with an endotherm in the DTA trace under N_2 (Fig. 1F). In the other samples, the gradual water loss over a wide temperature range explains the lack of sharp dehydroxylation endotherms in the DTA traces. In some respects these TG curves are similar to those for nontronite [11], which loses ~10% interlayer water below 150°C and ~4% hydroxyl water between 300 and 700°C; the present high-temperature process is more gradual, however, and represents a 10—12% weight loss. The distinction between

structural hydroxyl water and mechanically-held water is therefore less clear in hisingerite, although the comparable weight losses for all samples may not be completely fortuitous, and could argue some degree of common structural organization within the samples.

The thermal analysis curves for the hisingerites bear resemblances to those for nontronite [11], particularly with respect to the diagnostic endotherm at 350—480° C. There is less similarity with the thermal behaviour of saponite, in which rather higher temperatures are recorded for the loss of both interlayer water (179—240° C) and hydroxyl water (~900° C) [19], although these endotherm temperatures are lowered to 120 and 700° C in iron-rich samples [15]. Typical weight losses in saponites (~10—17% below 105° C and 6—12% above 105° C) are similar to both hisingerite and nontronite. The DTA traces of muscovite and hydromuscovite are influenced by the particle size, but the main feature is a prominent endotherm at 750—900° C [19], not present in hisingerite. The associated weight loss (~4% up to 400° C, ~2% at 400—600° C) is also much less than in hisingerite. Interstratified montmorillonite/chlorite, another structural type suggested for hisingerite [4], shows two endotherms in the DTA trace [19], the larger (at ~610° C) corresponding to chlorite dehydroxylation and the smaller (at ~700° C) to montmorillonite dehydroxylation. A marked exotherm at 890° C is also due to chlorite decomposition [19]. Thus the thermal behaviour of the present

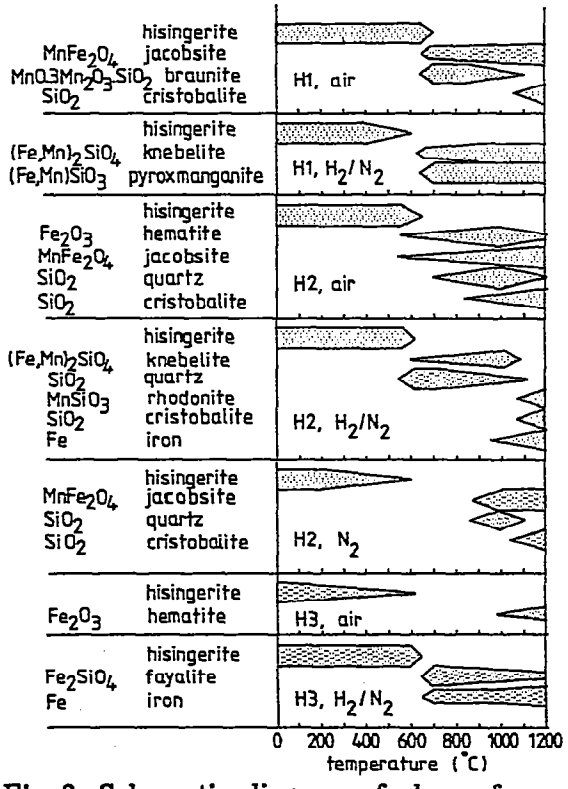

Fig. 3. Schematic diagram of phases formed from hisingerites as a function of temperature under various atmospheres.

hisingerites is more consistent with that of a smectite than with the other suggested structural types.

X-Ray diffraction

The phase compositions of the three samples as a function of temperature under various atmospheres are shown in Fig. 3. In samples H1 and H2, the broad hisingerite band at ~2.6 Å shifts slightly during heating at lower temperatures, later becoming the major jacobsite peak at ~650° C. Several other small sharp peaks, possibly associated with the chlorite impurity (in H1) or with manganese hydroxysilicates (in H2), develop slightly and undergo various intensity changes at temperatures below ~360° C, but have all disappeared by 400—600° C. Sample H2 fired in oxygen-free N_2 behaves identically. The peak at 7—8 Å in samples H1 and H3, attributed to a chlorite impurity, increases in intensity and broadens with increasing temperature, eventually disappearing abruptly at 650—700° C. The disappearance of the hisingerite spacings is concomitant with the appearance of new crystalline phases, except in sample H3 which remains X-ray amorphous from 650° C until the appearance of hematite at 900° C.

The nature of the crystalline products clearly depends on the composition of the starting material; manganese-containing samples form the spinel jacobsite ($MnFe_2O_4$) in air and nitrogen, the silica crystallizing as quartz or (at higher temperatures) cristobalite. In sample H2 the iron in excess of that required for jacobsite formation separates as hematite at ~650° C whereas in the low-manganese sample H3, hematite appears only above ~950° C and the silica component remains amorphous, evidenced by a broad diffraction hump at 3—4.5 Å. Amorphous SiO_2 similarly appeared in sample H2 in nitrogen between ~600° C and the appearance of crystalline quartz at ~880° C.

Under reducing conditions, the most common product is the ferrous olivine fayalite (Fe_2SiO_4), or, in the manganese-rich samples, the manganese-substituted analogue knebelite $(Fe, Mn)_2SiO_4$. At higher temperatures, the ferrous component of the knebelite in sample H2 is further reduced to the metal, resulting in the appearance of rhodonite ($MnSiO_3$); in sample H1, the analogous ferrous manganese pyroxene ferroan pyroxmanganite (Fe, Mn) SiO_3 is formed.

The X-ray behaviour of the heated hisingerites is not very different from that of nontronite [11], which after losing its hydration and hydroxyl water, also forms discrete oxides of iron and silicon in air or argon, and ferrous silicates in H_2/N_2. However, in nontronite, loss of interlayer water results in the formation of a dehydrate (sometimes called a dehydroxylate) phase, from which the crystalline products eventually are formed [11]. The X-ray pattern of the dehydrate is very similar to nontronite except that the basal spacing is collapsed to ~10 Å. Because no basal spacing is observed in hisingerite, this criterion cannot be applied; however, juxtaposition of the X-ray and TG results indicates that the non-basal hisingerite X-ray pattern persists up to about 600° C in all three samples, and disappears only when all the tightly-bound water is lost. Thus, the phase which exists between ~130 and 600° C

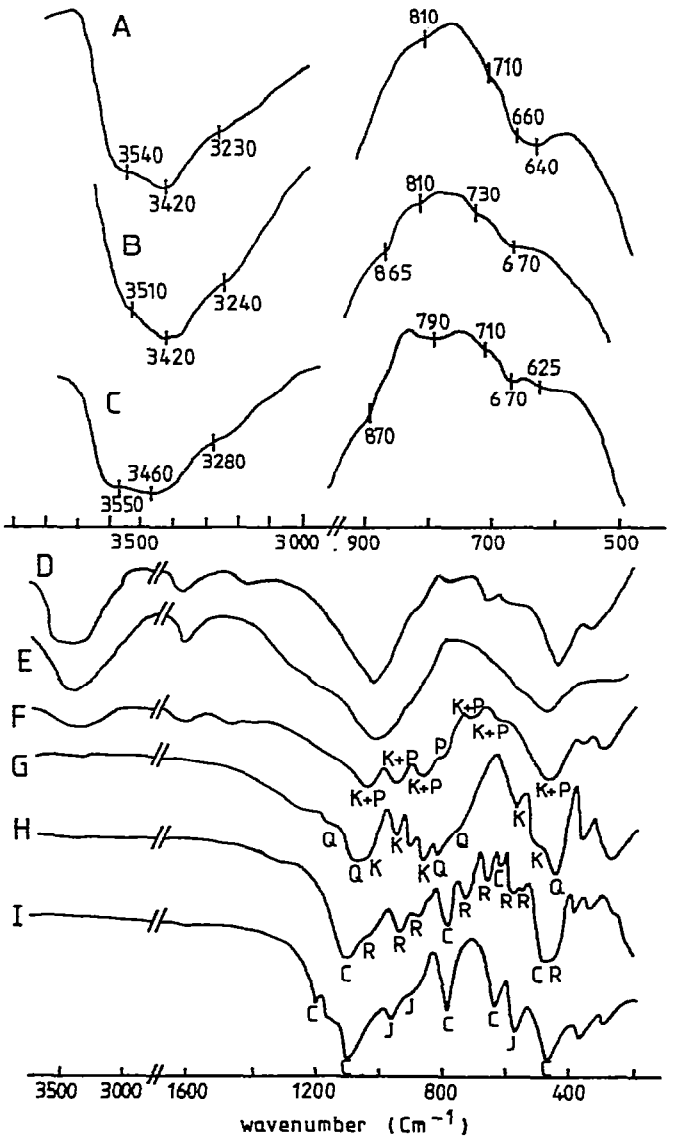

Fig. 4. Typical IR spectra of heated and unheated hisingerites. (A) Sample H3, unheated; (B) sample H2, unheated; (C) sample H1, unheated; (D) sample H1, unheated, whole spectrum; (E) sample H1, 400°C, air; (F) sample H1, 640°C, H_2/N_2; (G) sample H2, 1000°C, H_2/N_2; (H) sample H2, 1200°C, H_2/N_2; (I) sample H1, 1200°C, air. K = knebelite, P = pyroxmanganite, Q = quartz, R = rhodonite, C = cristobalite, J = jacobsite.

might correctly be described as a dehydrate, since its loosely-held water is lost but it retains hisingerite X-ray spacings. The analogy with nontronite cannot be taken further because of the lack of crystalline ordering in hisingerite which militates against a clear distinction between interlayer and other types of water.

IR spectroscopy

Typical IR spectra of samples heated under various conditions are shown in Fig. 4, which alsc includes details of the three unheated samples shown on

an expanded scale. The general features of the unheated hisingerite spectra (Fig. 4A—C) are similar, and resemble previously published spectra [5—7,12, 13], showing broad bands at 3400—3500 cm^{-1} and 1610 cm^{-1} due to water, a characteristic Si—O stretching vibration at 1020 cm^{-1} and the Si—O deformation at 450 cm^{-1}. Of greater interest in determining the nature and degree of any structural ordering present are the weak bands at 500—900 cm^{-1}, since these are said [6] to be similar to those in the spectrum of nontronite, in which mineral they are probably due to metal—hydroxyl vibrations [11]. Expanded portions of the unheated spectra (Fig. 4A—C) show ill-defined features in this region, although the three samples are similar, and resemble the spectra of iron-containing layer-lattice hydrous silicates [20]. The two manganese-containing samples show a slight shoulder at 865—870 cm^{-1} which coincides with a nontronite band earlier described as an Si—O—Fe^{3+} vibration [14], but more recently assigned to an Si—O (apical) stretching mode [15]. The weak band at 790—810 cm^{-1} present in all samples may correspond with the main Fe^{3+}—Fe^{3+}—OH band occurring in nontronite at 818—827 cm^{-1}. In the hydroxyl stretching region, the partially-resolved bands at about 3420 and 3550 cm^{-1} appear similar to the hydroxyl bands in some nontronites [15], but their frequency is slightly lower in hisingerite. The shoulder at about 3240 cm^{-1} is due to hydration water.

Comparison of the unheated hisingerite spectra with that of saponite [21] in the region 500—900 cm^{-1} shows corresponding broad peaks in the latter at ~809, 692 and 655 cm^{-1}. A saponite band at 534 cm^{-1} not observed in hisingerite is thought [21] to be due to a Mg—O vibration, and would not be expected in low-Mg hisingerites. However, the saponite hydroxyl stretching frequencies (3711 and 3676 cm^{-1}) are characteristic of trioctahedral smectites [21] and are significantly higher than in nontronite and hisingerite. Again, there is almost no correspondence between the hisingerite spectra and those of muscovite micas [21] in the region 500—900 cm^{-1}, even allowing for the fact that some of the seven muscovite bands in this region are due to Al—O or Al—O—Si vibrations, and would therefore be absent or very weak in the present hisingerites. The hisingerite spectra are also dissimilar to muscovite in the hydroxyl stretching region. However, reasonable agreement is found between the hisingerite spectra and those of some iron-rich chlorites [21], which show OH librations at ~820, 750 and 660 cm^{-1}. Thus the unheated hisingerite spectra bear greater similarity to those of nontronites and high-iron chlorites than to saponites and muscovites.

Heating the hisingerites above room temperature produces in some cases an initial sharpening of the peaks at 600—860 cm^{-1}, followed by their broadening and gradual disappearance which is complete by ~400°C (Fig. 4E). In some cases, the 865—870 cm^{-1} peak appears more temperature stable than the other peaks of the group, supporting the suggestion [22] that a hydroxyl group is not directly involved in this vibration. The disappearance temperatures of the 600—960 cm^{-1} peaks are independent of reaction atmosphere, but depend on the starting material; sample H1 is particularly heat-sensitive, its 600—860 cm^{-1} peaks having gone by 200°C. The temperatures at which these peaks are lost from all hisingerites are lower than in nontronite [11], as would be expected for a less ordered structure. The thermal

behaviour of the hydroxyl stretching bands at 3400—3550 cm^{-1} is also different in nontronite, in which these bands decrease in intensity concomitantly with the loss of the peaks at 600—900 cm^{-1}. In hisingerite, the loss of these peaks is accompanied by only a slight reduction in the hydroxyl band intensities, which persist to considerably higher temperatures, suggesting that only a small fraction of the tightly-bound water is associated with the vibrational modes at 600—900 cm^{-1}. This argues a structural concept for hisingerite in which regions of better ordering coexist intimately with disordered material, which by its gel-like nature retains (and possibly re-absorbs) hydroxyl water over a wide temperature range.

The IR spectra of samples heated to higher temperatures (Fig. 4F—I) contain peaks which can all be assigned to the various phases known to be present, but in some cases, the IR method detects characteristic vibrations of some phases before they have become sufficiently concentrated or crystalline to be seen by X-ray diffraction, e.g. quartz was detected in sample H2 fired in nitrogen at 550°C, but could only be detected by XRD in samples heated above 850°C. In all other respects, however, the IR and X-ray results are in agreement.

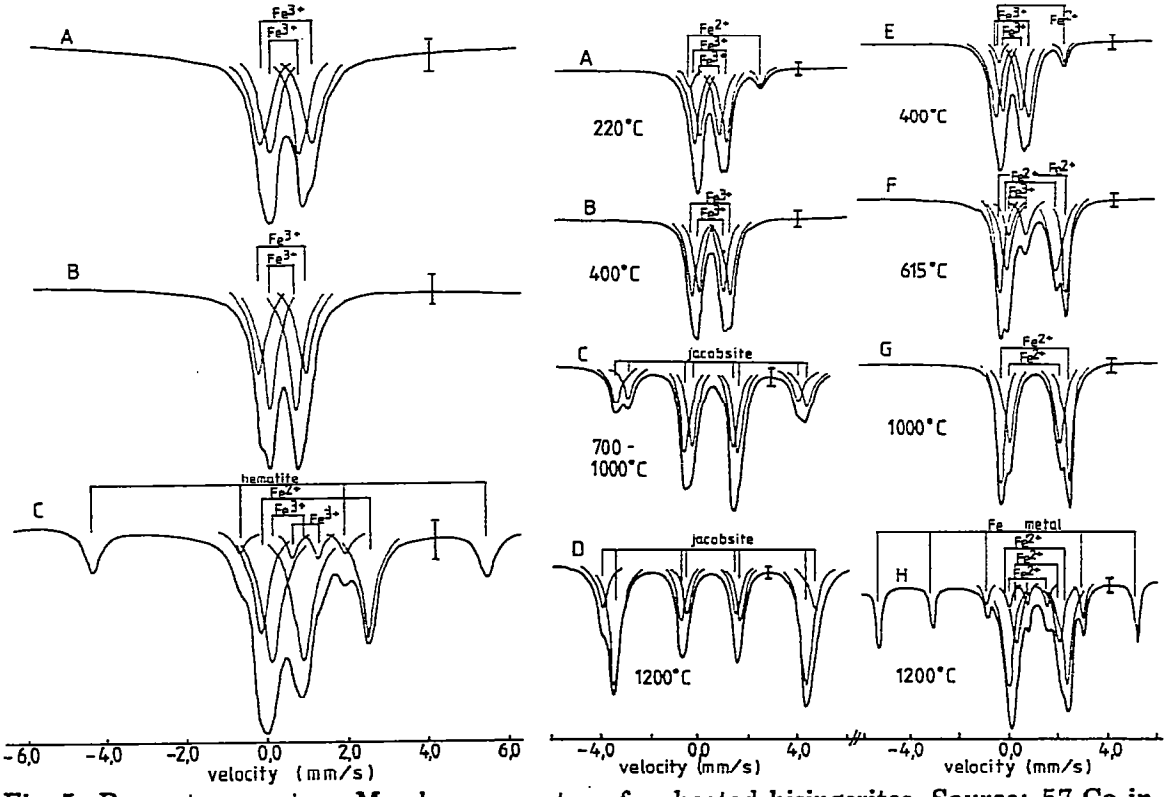

Fig. 5. Room-temperature Mossbauer spectra of unheated hisingerites. Source: 57-Co in Rh. (A) Sample H1; (B) sample H2; (C) sample H3.

Fig. 6. Typical room-temperature Mossbauer spectra of sample H1. (A—D) Heated in air; (E—H) heated in H_2/N_2.

TABLE 3

Mossbauer parameters for heated and unheated hisingerite (Six-line magnetic spectra omitted. Isomer shifts quoted with respect to natural iron)

Sample	Atmosphere	Temp. (°C)	I.S. (mm s^{-1})	Q.S. (mm s^{-1})	Assignment
H1	Air	Unheated	0.42	1.30	Fe^{3+},oh
			0.38	0.75	Fe^{3+},oh
		220—400	0.51—0.53	1.29—1.56	Fe^{3+},oh
			0.47—0.51	0.80—1.01	Fe^{3+},oh
		(220 only)	1.14	2.90	Fe^{2+}
	H_2/N_2	200—530	0.50—0.66	1.31—1.58	Fe^{3+},oh
			0.49—0.59	0.74—0.89	Fe^{3+},oh
			1.22—1.29	2.15—2.64	Fe^{2+}
		640—1000	0.61	0.68	Fe^{3+}
			1.23—1.31	2.68—2.75	Fe^{2+} Knebelite (M1)
			1.17—1.30	1.95—2.05	Fe^{2+} Knebelite (M2)
		1200	1.28	2.38	Fe^{2+} Ferroan
			1.30	1.75	Pyroxmanganite
			0.92	1.55	Fe^{2+} Td?
H2	Air	Unheated	0.41	1.17	Fe^{3+} oh
			0.41	0.65	Fe^{3+} oh
		200—850	0.47—0.51	1.14—1.49	Fe^{3+} oh
			0.46—0.51	0.70—0.91	Fe^{3+} oh
	N_2	250—550	0.46—0.52	1.36—1.42	Fe^{3+} oh
			0.46—0.51	0.81—0.87	Fe^{3+} oh
			0.92—1.02	2.64—2.86	Fe^{2+}

	H_2/N_2	200–550	0.46–0.52	1.34–1.51	Fe^{3+}
			0.45–0.62	0.80–0.90	Fe^{3+}
			1.21–1.25	2.44–2.46	Fe^{2+} } Incipient
		(550 only)	1.21	1.76	Fe^{2+} } knebelite
		615–1000	1.28–1.32	2.78–2.97	Fe^{2+} Knebelite (M1)
			1.24–1.29	1.95–2.04	Fe^{2+} Knebelite (M2)
		1200	1.33	2.47	} Fe^{2+}, Ferroan
			1.30	1.88	} Pyroxmanganite
			0.80	1.81	Fe^{2+}, Td?
H3	Air	Unheated	0.90	0.65	Fe^{3+},oh
			0.46	0.75	Fe^{3+},oh
			1.15	2.69	Fe^{2+}
		200–420	0.47–0.58	1.04–1.53	Fe^{3+}
			0.36–0.53	0.82–0.93	Fe^{3+}
		(not at 420)	1.02–1.15	2.69–2.93	Fe^{2+}
		540–650	0.65–0.71	1.11–1.16	Fe^{3+}
			0.42–0.48	1.01–1.11	Fe^{3+}
			0.19–0.24	1.11–1.20	Fe^{3+}
	H_2/N_2	200–450	0.59–0.65	0.89–1.03	Fe^{3+}
			0.38–0.45	0.76–0.87	Fe^{3+}
			1.04–1.20	2.52–2.73	Fe^{2+} Fayalite (M1)
		(450 only)	0.96	1.74	Fe^{2+} Fayalite (M2)
		700–1000	1.25–1.26	2.83–2.84	Fe^{2+} Fayalite (M1)
			1.14–1.26	2.08–2.19	Fe^{2+} Fayalite (M2)

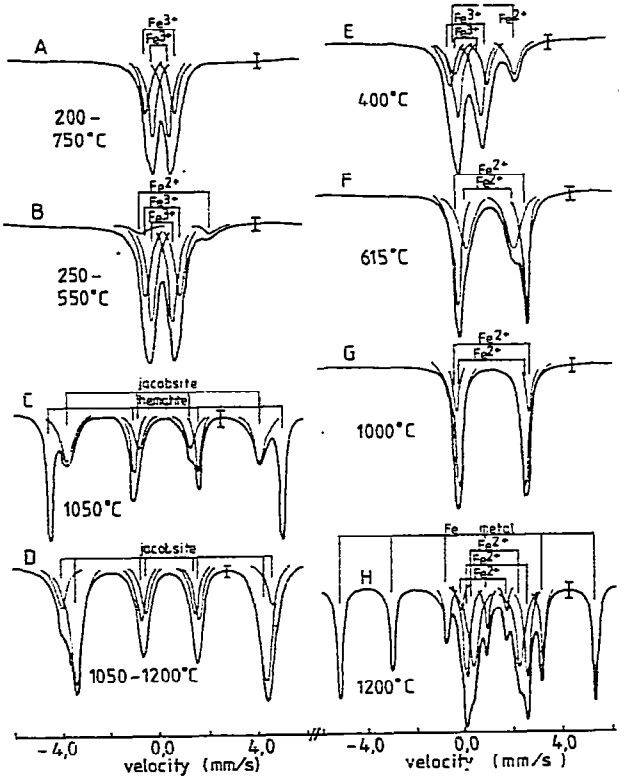

Fig. 7. Typical room-temperature Mossbauer spectra of sample H2. (A,C and D) Heated in air; (B and D) heated in N_2; (E—H) heated in H_2/N_2.

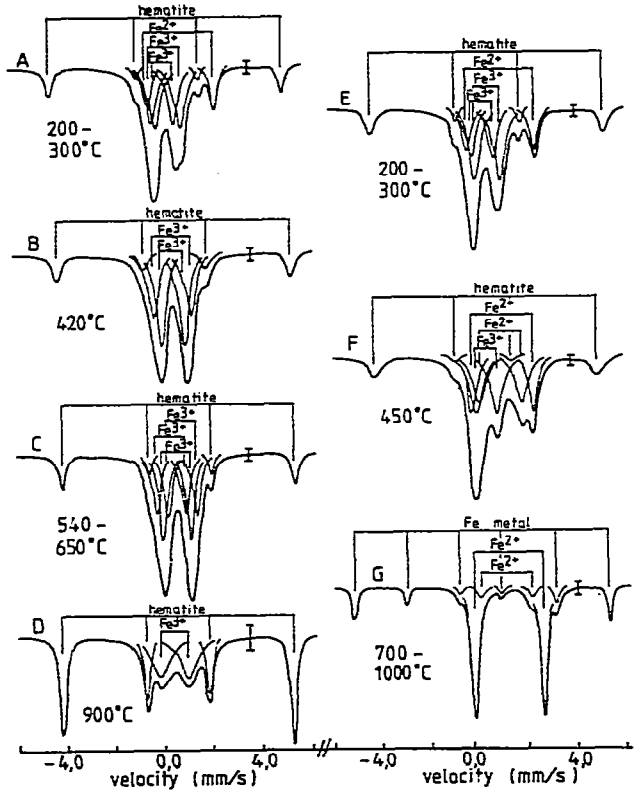

Fig. 8. Typical room-temperature Mossbauer spectra of sample H3. (A—D) Heated in air; (E—G) heated in H_2/N_2.

Mossbauer spectroscopy

Typical Mossbauer spectra of the heated and unheated hisingerites are shown in Figs. 5—8. The spectra of the unheated samples (Fig. 5) all show a broad ferric doublet which can be resolved by computer into at least two doublets, with parameters indicating octahedral sites (Table 3).

The ferric site in H1 and H2 with the smallest quadrupole splitting (Q.S) appears to correspond with one of the ferric sites in H3; the parameters of this site are of the same order as those recorded for several of the postulated structural-type-minerals, including an iron-rich saponite (I.S. = 0.36, Q.S. = 0.96 mm s^{-1}) [15], muscovites (I.S. = 0.36—0.46, Q.S. = 0.64—0.82) [23], the M2 sites of montmorillonites (I.S. = 0.27—0.36 *, Q.S. = 0.45—0.57) [24], and the sites in nontronite associated with *trans*-hydroxyl groups (I.S = 0.45—0.50, Q.S. = 0.60—0.67) [25]. The sites with higher Q.S. values observed in samples H1 and H2 have no parallel in the structural-type-minerals except perhaps for the M1 sites of montmorillonites (I.S. = 0.30—0.42 *, Q.S. = 0.85—1.22) [24]; these probably represent the more distorted octahedral sites. The range of sites distortions suggested by the hisingerite spectra are typical of a poorly crystalline or gel-like material. There is no indication in any of the hisingerites of sites similar to those ascribed to tetrahedral Fe^{3+} in nontronite (I.S. = 0.29—0.31, Q.S. = 0.47—0.61) [25]. The spectrum of sample H3 contains, in addition to the Fe^{3+} and hematite impurity, a significant ferrous doublet (Fig. 5C). The ferrous/ferric ratio in this material (disregarding the hematite) is estimated from the Mossbauer peak areas to be 0.59. The Fe^{2+} parameters in this sample are similar to those recorded in iron saponite (I.S. = 1.14, Q.S. = 2.52) [15] as well as in montmorillonites (I.S. = 1.06—1.11 *, Q.S. = 2.56—3.0) [24] and some muscovites (I.S. = 1.15 *, Q.S. = 3.02—3.04) [26]. Thus, the Mossbauer spectra of the unheated samples are generally consistent both with smectites and illites but cannot distinguish between the different structural possibilities.

On heating H1 in air, a small ferrous doublet develops at ~200°C (Fig. 6A), probably due to improved ordering of a ferrous site present in the original material rather than an unusual low-temperature reduction reaction. This ferrous site is completely oxidized by 400°C (Fig. 6B). Sample H2 shows a similar ferrous doublet when fired in N_2 at 220°C (Fig. 7B) which persists up to at least 550°C, preserving a constant ferrous/ferric ratio of ~0.08. Air-fired samples of H2 do not show this ferrous peak due to low-temperature oxidation. The significant ferrous peak present in unheated H3 slowly decreases on firing in air, and disappears completely by 420°C (Fig. 8).

Changes in the Mossbauer spectra below ~650° are of particular interest, to augment the poor X-ray data in this temperature range. The spectra of the air-fired samples can all be fitted by two ferric doublets, the relative proportions of which (estimated from the Mossbauer peak areas) change with firing temperature as shown in Fig. 9. If the ferric site having the smaller Q.S. is

* Isomer shift (I.S.) values recalculated and quoted here with respect to natural iron.

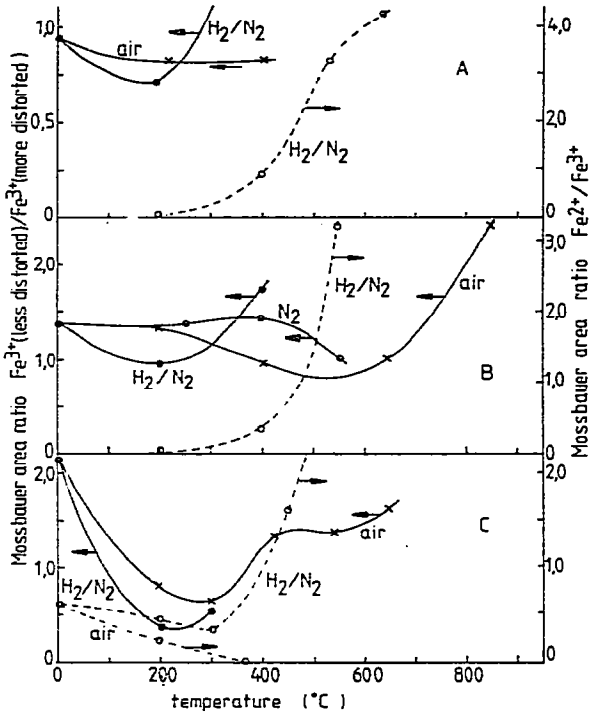

Fig. 9. Mossbauer ratios Fe^{2+}/Fe^{3+} and Fe^{3+} (less distorted)/Fe^{3+} (more distorted) as a function of temperature in various atmospheres. (A) Sample H1; (B) sample H2; (C) sample H3. The more distorted ferric sites are taken to be those with the larger Q.S. value.

identified as the less distorted from octahedral symmetry, Fig. 9 shows that in both air and H_2/N_2, the population of less distorted sites initially decreases, coinciding with the initial water loss, then increases as the more tightly bound water is removed and the structure approaches the point of recrystallization. Under reducing conditions, this increase in less distorted site population corresponds with the onset of reduction, as indicated by an increase in the ratio Fe^{2+}/Fe^{3+}, also plotted in Fig. 9. Such estimates of ferrous/ferric ratio assume negligible cosine smearing of the spectra and not too high an iron concentration per cm^2 of absorber area (thin samples), both of which conditions are satisfied here. The assumption that the recoil-free fraction is similar for Fe^{2+} and Fe^{3+} is also implicit in such ferrous/ferric determinations.

The ratio of less distorted to more distorted ferric sites for sample H3 in air (Fig. 9C) shows an inflexion over the temperature range 400—700° C, approximately coinciding with a prolonged X-ray amorphous state (Fig. 3). Over this temperature range, the ferric Mossbauer peaks broaden and become increasingly diffuse (Fig. 8C, D). At 540—650° C, the broadened spectra have been fitted to three ferric doublets; particular significance should not be attached to the additional doublet, however, as the system is probably best described as containing a number of rather ill-defined non-equivalent sites. By 900° C the ferric peaks can barely be distinguished (Fig. 8D).

The changes in the present hisingerite spectra over the temperature range at which water is lost bear similarities to the spectra of heated nontronites

[11], in which broadening and increasing distortion is noted prior to recrystallization. It is likely, however, that this is common behaviour in other hydrous iron minerals as well, and by itself does not constitute evidence of identity between hisingerite and nontronite.

Above 700°C, samples H1 and H2 heated in air and N_2 have spectra which can be fitted to four pairs of overlapping doublets (Figs. 6C, D, 7C, D), which at 1200°C become identical with the inner portion of the spectrum of jacobsite [27]. This spectrum has been described in terms of two overlapping six-line magnetic spectra, the outer arms of which lie outside the velocity range used here. At 1050°C, sample H2 passes through a stage at which the inner peaks of a six-line hematite spectrum can also be resolved (Fig. 7C).

Under reducing conditions, the higher-temperature spectra of all three samples can be fitted to two ferrous doublets with parameters similar to those of the M1 and M2 sites of the olivine fayalite [28] or a ferrous pyroxene [29]. Small differences in the parameters of the three samples (Table 3) are probably due to differences in the contents of manganese, which replaces Fe^{2+} in the olivine or pyroxene structure. At 1200°C, further reduction of the ferrous silicate results in the appearance of iron metal and an additional Fe^{2+} doublet of possibly tetrahedral symmetry.

Implications to the structure of hisingerite

The previously-suggested structural types of hisingerite can be summarized as (i) a dioctahedral smectite resembling nontronite, (ii) a trioctahedral smectite resembling an iron-rich saponite, (iii) an interstratified montmorillonite—chlorite, or (iv) a dioctahedral hydromica of the muscovite type. Chemical analyses of the present samples can be fitted by either smectite or hydromica models; the unit cell contents based on a smectite have octahedral site occupancies intermediate between dioctahedral and trioctahedral, but probably closer to the latter. Samples H2 and H3 are reasonably well fitted by a hydromuscovite formula but H1 has too many octahedral ions to be properly accommodated by a hydromuscovite structure; further, a hydromuscovite structure is not supported by thermal analysis or IR evidence.

Dioctahedral and trioctahedral smectite models are equally compatible with the DTA, TG and Mossbauer results but the IR spectra in the hydroxyl stretching region are more consistent with nontronite than saponite. The X-ray patterns are also more consistent with nontronite (except for the lack of a basal spacing). The phase changes on heating are similar to those of nontronite, but may represent behaviour common to hydrated systems containing iron and silica in intimate association (cf. the thermal behaviour of synthetic co-precipitated iron—silicon hydroxide [30].

The possibility of an interstratified structure containing chlorite cannot be eliminated by the present results; the intimate association of chlorite with sample H3 has previously been demonstrated [4] and is probably the source of the ferrous Mossbauer spectrum in that sample. However, there is no evidence that chlorite is an essential component of all hisingerites.

The weight of evidence therefore suggests that the present samples are very poorly crystalline materials in which exist elements of a smectite struc-

ture. Compositional variability and incorporation of other iron and manganese-rich phases make it impossible to distinguish between dioctahedral and trioctahedral structures on the basis of chemical analyses, but other evidence points to dioctahedral rather than trioctahedral characteristics. The lack of a smectite basal spacing in many hisingerites, including the present samples, is probably related to a lack of stacking periodicity consequent on the high ferric iron content, but may also be influenced by the mode of occurrence (i.e. whether from smectite weathering or co-precipitation) [6].

CONCLUSIONS

Thermal analysis, X-ray diffraction, IR and Mossbauer spectroscopy suggest that the present hisingerites contain elements of poorly crystalline structure with similar characteristics to nontronite. Although chlorite occurs in one of the samples, it is not an essential component of all hisingerites. The absence of a nontronite basal spacing reflects poor stacking order due to high ferric iron content.

On heating, the hisingerites lose 10—12% loosely-bound water below 120°C followed by a slower 8—10% loss up to ~600°C, the temperature at which crystalline products are formed. In air, the products are iron oxide or mixed iron—manganese oxides (depending on the initial composition) and SiO_2. Under reducing conditions, reduction sets in at 200—300°C, becoming rapid at 500—600°C; the crystalline products are ferrous and ferro-manganese silicates of olivine or pyroxene type, again depending on initial composition. Changes in the Mossbauer spectra on heating indicate that progressive removal of water is accompanied by an initial increase in the population of less distorted ferric sites followed by a progressive increase in distortion up to the point of recrystallization.

ACKNOWLEDGEMENTS

We are indebted to Dr. P.E. Desautels, Smithsonian Institution, Washington, for providing sample H2 and to Dr. B. Lindqvist, University of Uppsala, Sweden, for samples H1 and H3. The chemical analyses were by J.E. Patterson and A. Cody. We are also grateful to Dr. D.M. Bibby for assistance with the DTA work, Dr. N.B. Milestone for assistance with the TG work and Dr. L.P. Aldridge for assistance with the use of his Mossbauer programme.

REFERENCES

1 E.S. Dana, Descriptive Mineralogy, Wiley, New York, 6th edn., 1892, p. 702.
2 T. Sudo and T. Nakamura, Am. Mineral., 37 (1952) 618.
3 R.V. Dietrich, Nor. Geol. Tidsskr., 41 (1961) 95.
4 B. Lindqvist and S. Jansson, Am. Mineral., 47 (1962) 1356.
5 G.A. Golubova, T.N. Grigor'eva, I.V. Nakolaeva and M. Shcherbakova, Primen. Mol.

Spektrosk. Khim., Sb. Dokl. Sib. Soveshch., 3rd, Krasnoyarsk, U.S.S.R., 1964, p. 263.
6 N. Kohyama and T. Sudo., Clays Clay Miner., 23 (1975) 215.
7 J.A. Whelan and S.S. Goldich, Am. Mineral., 46 (1961) 1412.
8 J.W. Gruner, Am. Mineral., 20 (1935) 475.
9 G.M. Schwartz, Am. Mineral., 9 (1924) 142.
10 S.H.U. Bowie, Bull. Geol. Surv. G.B., 10 (1955) 45.
11 K.J.D. MacKenzie and D.E. Rogers, Thermochim. Acta, 18 (1977) 177.
12 A.M. Clark, A.J. Easton, G.C. Jones and M. Mount, Mineral. Mag., 42 (1978) M. 26.
13 A.I. Soklakov and M.D. Dorfman, Tr. Mineral. Muz., Akad. Nauk S.S.S.R., 15 (1964) 167.
14 T. Sudo, J. Geol. Soc. Jpn., 60 (1954) 18.
15 N. Kohyama, S. Shimoda and T. Sudo, Clays Clay Miner., 21 (1973) 229.
16 W.A. Deer, R.A. Howie and J. Zussman, Rock-Forming Minerals, Vol. 3, Longmans, London, 1962, p. 218.
17 C.S. Ross and S.B. Hendricks, U.S. Geol. Surv., Prof. Pap. 205B (1945).
18 G. Brown and K. Norrish, Mineral. Mag., 29 (1952) 929.
19 R.C. MacKenzie (Ed.), The Differential Thermal Investigation of Clays, Miner. Soc. Monogr., London, 1957.
20 V. Stubican and R. Roy, J. Am. Ceram. Soc., 44 (1961) 625.
21 V.C. Farmer (Ed.), The Infrared Spectra of Minerals, Miner. Soc. Monogr., London, 1974.
22 J.D. Russell, B.A. Goodman and A.R. Fraser, Clays Clay Miner., 27 (1979) 63.
23 H. Annersten and U. Halenius, Am. Mineral., 61 (1976) 1045.
24 I. Rozenson and L. Heller-Kallai, Clays Clay Miner., 25 (1977) 94.
25 B.A. Goodman, J.D. Russell, A.R. Fraser and F.W.D. Woodhams, Clays Clay Miner., 24 (1976) 53.
26 C.S. Hogg and R.E. Meads, Mineral. Mag., 37 (1970) 606.
27 (a) H. Yasuoka, A. Hirai, T. Shinjo, M. Kiyama and Y. Bando, J. Phys. Soc. Jpn. 22 (1967) 174.
(b) G.A. Sawatzky, F. Vander Woude and A.H. Morrish, Phys. Lett. A, 25 (1967) 147.
28 W.R. Bush, S.S. Hafner and D. Virgo, Nature (London), 227 (1970) 1339.
29 E.K. Dowty and D.H. Lindsley, Am. Mineral., 58 (1973) 850.
30 V.F. Kovtun, Yu. A. Taran and I.O. Moskalik, Russ. J. Phys. Chem., 40 (1966) 77.